

RealCamo: Boosting Real Camouflage Synthesis with Layout Controls and Textual-Visual Guidance

Chunyuan Chen¹ Yunuo Cai² Shujuan Li¹ Weiyun Liang¹ Bin Wang¹ Jing Xu¹

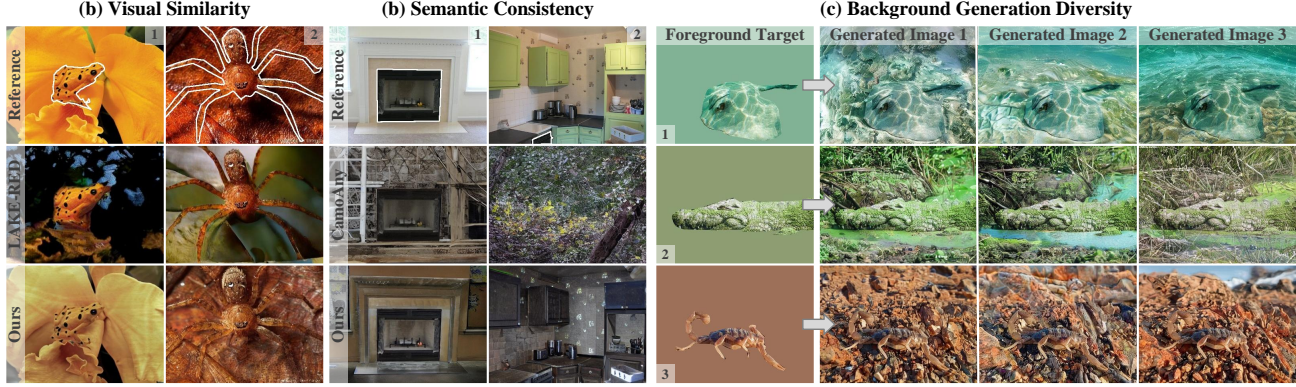


Figure 1. Motivation and qualitative comparison of camouflaged image synthesis. (a) **LAKE-RED** (Zhao et al., 2024) fails to achieve effective camouflage, with targets remaining visually distinguishable, whereas our method produces images with well-camouflaged targets. (b) **CamoAny** (Das & Gopalakrishnan, 2025) achieves visual camouflage but suffers from weak semantic consistency between the target and the generated background, in contrast, our method preserves semantic coherence, resulting in more realistic scenes. (c) **Our approach** is capable of generating diverse and realistic camouflaged images while jointly satisfying visual similarity and semantic consistency.

Abstract

Camouflaged image generation (CIG) has recently emerged as an efficient alternative for acquiring high-quality training data for camouflaged object detection (COD). However, existing CIG methods still suffer from a substantial gap to real camouflaged imagery: generated images either lack sufficient camouflage due to weak visual similarity, or exhibit cluttered backgrounds that are semantically inconsistent with foreground targets. To address these limitations, we propose ReamCamo, a unified out-painting based framework for realistic camouflaged image generation. ReamCamo explicitly introduces additional layout controls to regulate global image structure, thereby improving semantic coherence between foreground objects and generated backgrounds. Moreover, we construct a multi-modal textual–visual condition by combining a unified fine-grained textual task description with texture-oriented background retrieval, which jointly guides the generation pro-

cess to enhance visual fidelity and realism. To quantitatively assess camouflage quality, we further introduce a background–foreground distribution divergence metric that measures the effectiveness of camouflage in generated images. Extensive experiments and visualizations demonstrate the effectiveness of our proposed framework.

Code and results will be released soon.

1. Introduction

Why Synthesize Data: Concealed visual perception tasks, exemplified by camouflaged object detection (COD) (He et al., 2025), aim to identify semantically meaningful targets that are visually indistinguishable from their surrounding backgrounds. Such tasks are increasingly important in real-world applications, including medical diagnosis, agricultural and industrial production (Xiao et al., 2024). Despite recent progress, the development of COD remains fundamentally constrained by the limited scale of available training data.

In contrast to large-scale benchmarks for general object detection & segmentation, such as PASCAL VOC (Everingham et al., 2010) and MS-COCO (Lin et al., 2014), which contain tens to hundreds of thousands of precisely annotated images, existing COD datasets (Fan et al., 2020; Lv et al.,

¹College of Artificial Intelligence, Nankai University, Tianjin, China ²School of Data Science, Fudan University, Shanghai, China. Correspondence to: Jing Xu <xujing@nankai.edu.cn>.

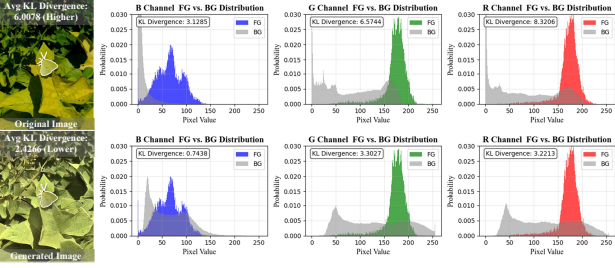


Figure 2. The proposed KL divergence based metric. Existing generative evaluation metrics, such as FID and KID, are insufficient to measure the similarity between foreground and background, while our proposed KL_{BF} provides a quantitative assessment of camouflage. **Top:** Image with a higher KL_{BF} . **Bottom:** Our generated image with a lower KL_{BF} , more camouflaged.

2021) typically comprise only a few thousand samples. This scarcity arises from two intrinsic challenges: **(i)** camouflaged objects are inherently difficult to annotate due to its high visual similarity to backgrounds, and **(ii)** camouflaged scenes with high quality are themselves rare and costly to capture in the real world. As a result, data insufficiency has become a critical bottleneck for improving both the robustness and generalization of COD models.

Recent advances in image generation models, including GAN (Goodfellow et al., 2020) and diffusion models (Ho et al., 2020; Rombach et al., 2022), offer a promising alternative, while leveraging high-quality synthetic data to augment training has been shown to be an effective and cost-efficient strategy in multiple vision tasks such as salient object detection (Kupyn et al., 2025). This observation motivates the camouflaged image synthesis task, whose core objective is to generate realistic and diverse camouflaged scenes that can meaningfully complement limited real-world datasets and thereby improve downstream COD performance.

Why Out-Painting: Existing approaches to camouflaged image synthesis can be broadly categorized into two paradigms. The first paradigm, exemplified by style-transfer based methods such as LCGNet (Li et al., 2022b), modifies the appearance of a target object to match a given background. However, this process often alters object-specific textures and visual cues to such an extent that the semantic identity of the target is partially or entirely compromised. Consequently, these methods achieve camouflage by enforcing visual uniformity, rather than by modeling the natural interaction between an object and its environment.

The second paradigm, represented by out-painting based methods such as LAKE-RED (Zhao et al., 2024), follows a fundamentally different strategy. Instead of altering the target object, these methods preserve its semantic content and generate surrounding background regions whose textures and structures are consistent with the target appearance. This formulation enables camouflage to emerge from context

tual compatibility between the object and its environment, rather than from direct manipulation of the object itself.

Compared with style-transfer based approaches, out-painting offers several advantages. First, it maintains the semantic integrity of the target while avoiding the need for an externally provided background image. More importantly, it aligns more closely with the natural principles of camouflage observed in the real world. Camouflage is inherently a relative and environment-dependent phenomenon: the same object may appear well camouflaged in one context but highly salient in another (Wang et al., 2025). From the perspective of natural selection, creatures do not actively redesign their appearance to match each environment, instead, environmental variation favors the survival of individuals whose appearances are already compatible with their surroundings. This perspective naturally corresponds to the out-painting formulation.

Why Background Control: For out-painting based methods to produce realistic and effective camouflaged training data, we argue that two key requirements must be simultaneously satisfied. First, the generated background should exhibit strong appearance compatibility with the target, particularly in terms of color distribution and texture patterns, so that the target is genuinely camouflaged under visual perception. Second, the background must convey semantically plausible content consistent with real-world priors, for instance, aquatic objects should appear in water rather than in visually incompatible contexts.

Meeting these requirements is inherently challenging because camouflaged targets typically occupy only a small spatial region of the image. Consequently, out-painting methods must synthesize large background areas with limited target-conditioned information, often leading to a trade-off between visual similarity and semantic consistency. As shown in Fig. 1 (a & b), existing approaches exhibit clear deficiencies: some generated backgrounds that are insufficiently compatible with the target appearance, resulting in weak camouflage, while others produce visually plausible textures that lack coherent or meaningful semantics.

These limitations indicate that unconstrained out-painting is inadequate for high-fidelity camouflaged image generation. To address this issue, explicit guidance and control mechanisms during background synthesis are essential, enabling the generation process to balance appearance-level camouflage with semantic realism.

Our Focus and Contributions: Based on the above analysis, this work focuses on three tightly coupled contributions:

(1) Controlled camouflaged image synthesis. To overcome the limitations of existing out-painting based methods in background generation, we introduce a unified out-painting based framework termed **RealCamo**, which integrates ex

plastic layout controls and textual-visual guidance. We argue that background layout plays a critical role in determining semantic plausibility. Building upon the contrast control in CamoAny, we incorporate additional depth and holistically-nested edge information into ControlNet to explicitly constrain the spatial layout of generated scenes, thereby preserving semantic realism. Furthermore, to enhance camouflage effectiveness at the texture level, we propose a textual-visual guidance mechanism that combines a unified fine-grained textual task descriptions with additional visual cues retrieved according to target texture characteristics, enhancing visual fidelity and realism of generation.

(2) Camouflage effectiveness evaluation metrics. A realistic camouflaged image should preserve the original scene layout while achieving camouflage through modifications in background color and texture. Existing generative evaluation metrics, such as FID and KID, are insufficient to capture this requirement. We therefore introduce SSIM to quantify structural consistency between generated and original images as a indicator for semantic realism. In addition, we propose a KL divergence based metric KL_{BF} , which measures the similarity between background and foreground pixel distributions, providing a principled quantitative assessment of camouflage effectiveness, as shown in Fig. 2.

(3) Downstream evaluation. To assess the practical utility of the generated camouflaged images, we construct a large-scale synthetic dataset, **SynCOD12K**, as supplementary training data for camouflaged object detection. Extensive experiments on four COD benchmarks demonstrate consistent performance improvements, with further investigations on the effects of camouflage-augmented data on related salient and general object detection tasks.

2. Related Work

Synthetic Dataset Generation. Synthetic data has become an effective strategy for alleviating data scarcity in computer vision (Mumuni et al., 2024). Advances in generative models, including GANs and diffusion models, have enabled the construction of large-scale, high-quality synthetic datasets. DatasetGAN (Zhang et al., 2021) generates image-annotation pairs by exploiting the latent feature space of pretrained GANs, while BigDatasetGAN (Li et al., 2022a) extends this paradigm to ImageNet-scale class diversity using VQGAN (Esser et al., 2021). More recently, diffusion-based methods such as DiffuMask (Wu et al., 2023a) and DatasetDM (Rombach et al., 2022) leverage text-to-image models to produce photorealistic images and corresponding annotations for downstream perception tasks. Despite their success, these approaches primarily focus on generic image synthesis and annotation, and remain limited when applied to structurally complex and semantically subtle scenarios such as camouflaged image generation.

Camouflaged Image Generation. Camouflaged image generation, introduced by Chu et al. (2010), can be categorized into two paradigms: **Style transfer based background-guided** approaches modify foreground appearance to blend targets into given backgrounds. DCI (Zhang et al., 2020) employs an attention-aware camouflage loss to suppress salient cues while preserving subtle perceptual features, and LCGNet (Li et al., 2022b) achieves extreme camouflage by fusing high-level foreground and background representations. In contrast, **out-painting based foreground-guided methods** generate backgrounds conditioned on the foreground target. LAKE-RED (Zhao et al., 2024) introduces a knowledge retrieval-augmented framework using a pretrained codebook, while FACIG (Chen et al., 2025) refines feature integration to reduce foreground distortion. CamoAny (Das & Gopalakrishnan, 2025) further improves background synthesis through controlled out-painting and representation engineering. Despite these advances, existing methods still struggle to simultaneously achieve strong visual similarity and semantic consistency. More recently, the text-driven method CT-CIG (Qian et al., 2025) has shown promise in realistic camouflage synthesis, but the inability to provide aligned annotations limits their applicability to downstream camouflaged object detection applications.

Controlled Image Generation. Recent advances in text-to-image (T2I) generation integrate large-scale text encoders, such as CLIP (Kim et al., 2021) and T5 (Raffel et al., 2020), into diffusion models, yielding powerful T2I models. To enable fine-grained spatial control, ControlNet (Agrawala, 2023) introduces an auxiliary trainable branch to inject conditional signals into pretrained diffusion models. Building upon this design, UniControl (Qin et al., 2023) employs a task-aware hypernetwork to modulate zero convolutions of the ControlNet in handling multiple conditions, while CtrLoRA (Xu et al., 2025) further reduces parameter overhead through condition-specific LoRA (Hu et al., 2022) fine-tuning, and Sharma et al. (2025) proposes an N-channel ControlNet to improve object preservation, prompt alignment, and aesthetic quality under multiple control settings.

3. Methodology

3.1. Preliminary

Our proposed method is based on the classic Latent Diffusion Models (LDMs) (Rombach et al., 2022) and ControlNet (Agrawala, 2023). Here, we briefly revisiting their basics, with more details can be found in Appendix B.

Latent Diffusion Models. LDMs generate high-quality images by reversing a Markov forward process in the latent space. Specifically, Given a VAE (Rezende et al., 2014) with encoder \mathcal{E} and decoder \mathcal{D} , Gaussian noise ϵ is progressively added to a latent representation $z_0 = \mathcal{E}(x_0)$ of the original

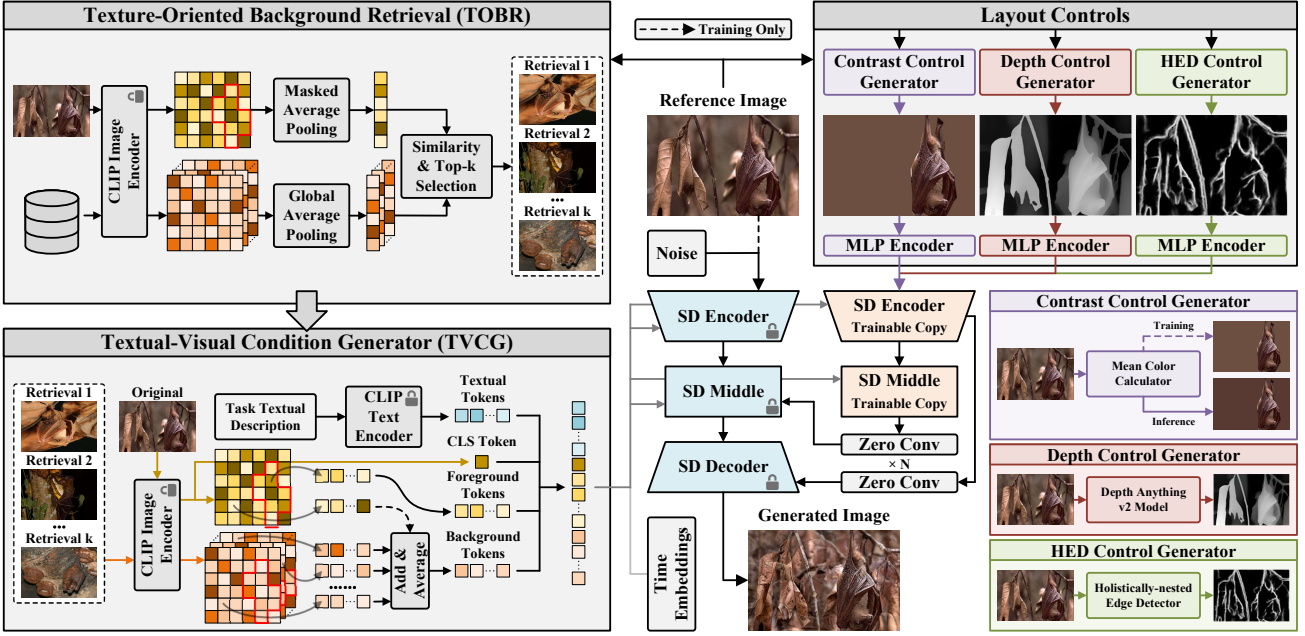


Figure 3. The pipeline of our camouflaged image generation framework RealCamo. Explicit layout controls (*i.e.*, the contrast, depth, and HED controls) are extracted by the **Layout Controls Generator** (LCG) and injected to ControlNet, while the multi-modal condition produced by the **Textual-Visual Condition Generator** (TVC) is used as a guidance in refining the camouflage generation process.

image x_0 , resulting in a noisy image $z_t = \alpha_t z_0 + (1 - \alpha_t) \epsilon$, with more noise being introduced when α_t decreases as timestep t increases. A denoising network ϵ_θ is trained to predict the added noise given a condition c^t following:

$$\mathcal{L} = \mathbb{E}_{x_0, t, \epsilon \sim \mathcal{N}(0, I), \mathcal{E}} [\| \epsilon - \epsilon_\theta(z_t, t, c^t) \|], \quad (1)$$

and reverse the noise image to a latent representation z'_0 , which is finally decoded into the image space by $\mathcal{D}(z'_0)$.

ControlNet. ControlNet extends the structural controllability of LDMs by incorporating addition conditions (c^f) like Canny edges and human pose. With the introduction of additional trained branch aided by zero convolutions, ControlNet reformulates Equation 1 as:

$$\mathcal{L} = \mathbb{E}_{x_0, t, c^f, \epsilon \sim \mathcal{N}(0, I), \mathcal{E}} [\| \epsilon - \epsilon_\theta(z_t, t, c^t, c^f) \|_2^2], \quad (2)$$

which enables fine-grained spatial control during generation.

3.2. Framework Overview

As illustrated in Fig. 3, the proposed **RealCamo** framework is built upon Stable Diffusion 1.5 (Rombach et al., 2022) and ControlNet (Agrawala, 2023), enabling controllable camouflaged image generation through complementary structural and semantic conditioning. Control signals are injected in two ways: **(i)** structural constraints introduced via ControlNet to regulate spatial layout, and **(ii)** multi-modal prompts injected through cross-attention to guide image content. These mechanisms align with our objective that high-quality camouflage requires both **visual similarity** and **semantic**

consistency between foreground targets and background scenes. Accordingly, we employ a **Layout Controls Generator** to provide explicit structural priors via ControlNet, and a **Textual-Visual Condition Generator** that integrates a unified fine-grained task description with background images retrieved by a **Texture-Oriented Background Retrieval** module, producing informative multi-modal prompts to effectively steer the camouflage generation process.

3.3. Layout Controls Generator

We argue that semantic consistency in camouflaged image generation is largely determined by the structural layout of the image. Prior methods (Zhao et al., 2024; Das & Gopalakrishnan, 2025) often yield cluttered or physically implausible backgrounds due to the lack of explicit layout constraints. To address this, we propose a layout conditions generator (LCG) that extracts complementary structural cues and injects them via ControlNet, as shown in Fig. 3. Specifically, for a given image I and a corresponding mask M which indicate the foreground target, we employ LCG to extract **contrast**, **depth**, and **holistically-nested edge (HED)** controls as explicit structural priors to promote coherent spatial organization and improved foreground–background semantic alignment:

$$c_{cst}, c_{dep}, c_{hed} = LCG(I, M, is_training). \quad (3)$$

Each control signal is embedded using a dedicated MLP (Qin et al., 2023) due to distributional differences, and then fused as a structural guidance for ControlNet to process.

Contrast Control. Following Das & Gopalakrishnan (2025), contrast control c_{cst} aims to preserve the foreground target while providing basic regulation of color contrast, varies when training and inference based on *is_training*.

Depth Control. Depth control c_{dep} is generated using Depth Anything V2 (Yang et al., 2024), and is intended to constrain the spatial relationships within the image.

HED Control. HED control c_{hed} is obtained by deploying Holistically-nested edge detection (Xie & Tu, 2015) to regulate the contours of the main elements in the image.

3.4. Texture-Oriented Background Retrieval

Compared to generic image synthesis, camouflaged image generation requires backgrounds that are quite complex and sometimes unconventional. Although LAKE-RED (Zhao et al., 2024) retrieves background embeddings from a pre-trained codebook, such representations learned from generic image distributions lack camouflage-specific priors. We therefore introduce a texture-oriented background retrieval (TOBR) module that uses camouflaged images as a domain-specific background knowledge base. As illustrated in Algorithm 1, given a target foreground object, a CLIP image encoder is adopted to extract texture-aware features for the object and all candidates in the knowledge base, with the top- k most similar images in the embedding space are retrieved and then incorporated into multi-modal prompt construction to guide the camouflage generation process.

3.5. Textual-Visual Condition Generator

Textual conditioning is central to T2I generation. Although Das & Gopalakrishnan (2025) enhances textual prompts via prompt engineering, the incorporated background semantics remain limited. While detailed scene descriptions have been shown to improve the realism of camouflaged image synthesis (Qian et al., 2025), acquiring scene-specific fine-grained descriptions is often labor-intensive. We therefore propose a textual-visual condition generator (TVCG) that constructs a multi-modal prompt by combining a unified fine-grained task description with high-quality background visual embeddings. This design offers richer guidance for generation and improves visual similarity between the foreground target and the background. The multi-modal prompt comprises three components: (i) fine-grained textual task description, (ii) object category information, and (iii) reference background visual cues.

Fine-Grained Textual Task Description. Instead of using overly simplistic prompts (e.g., “*image of a fish Camouflaged with Background*” (Das & Gopalakrishnan, 2025)) or labor-intensive, scene-specific descriptions (e.g., “*A fish with mottled green and brown patterns and elongated appendages in a coral reef ecosystem.*” (Qian et al., 2025)),

Algorithm 1 Texture-Oriented Background Retrieval

Input: image I, mask M, knowledge base with K candidates $B = \{S_i\}_{i=1}^K$, number of retrieval samples k
Initialize: similarity scores $S = \emptyset$, retrieval samples $R = \emptyset$, target $E_t = \text{MaskedAvgPool}(\text{CLIP}_I(I), M)$
for $i = 1$ **to** K **do**
 sample $E_i = \text{GlobalAvgPool}(\text{CLIP}_I(S_i))$
 score $R_i = \text{CosineSimilarity}(E_t, E_i)$, $S \leftarrow R_i$
end for
for $j = 1$ **to** k **do**
 index $x = \text{ArgMax}(S)$, $R \leftarrow S_x$
 remove S_x **from** S
end for
Return: retrieval samples $R = \{S_j\}_{j=1}^k$

we adopt a unified fine-grained textual task description “*A realistic image of an object blending into its surroundings, where the background shares similar colors, textures, and patterns with the object, making it hard to distinguish. Natural lighting, photorealistic, seamless camouflage, high detail.*” as the textual guidance in generation. This unified description improves generation quality while eliminating the need for manually crafting scene-specific prompts, and is encoded into textual tokens c_{tex} via a CLIP text encoder.

Object Category Information. For the given image, we adopt the [CLS] token processed by a CLIP image encoder as a compact category representation of the foreground object, avoiding explicit class identification while preserving informative semantic guidance.

Reference Background Visual Cues. To provide richer background guidance for the camouflage generation process, we incorporate the samples retrieved by TOBR as visual reference knowledge into the multi-modal prompt. Specifically, we employ a CLIP image encoder to extract visual embeddings from the input image I and its top- k TOBR-retrieved samples $\{S_j\}_{j=1}^k$. Guided by the foreground mask M, the foreground region of the input image is preserved, while the background regions are fused with the retrieved visual knowledge to construct background-aware visual cues c_{vis} . This process can be formulated as:

$$e_t = \text{CLIP}_I(I), \quad e_j = \text{CLIP}_I(S_j), \quad j = 1, 2, \dots, k, \quad (4)$$

$$c_{vis} = \begin{cases} e_t \cdot M + \frac{1}{k+1} \cdot (e_t + \sum_{j=1}^k e_j) \cdot (1 - M), & \text{if training} \\ e_t \cdot M + \frac{1}{k} \cdot \sum_{j=1}^k e_j \cdot (1 - M), & \text{if inference.} \end{cases} \quad (5)$$

The final multi-modal conditional prompt is the concatenation of c_{txt} , c_{cls} , and c_{vis} along the sequence dimension.

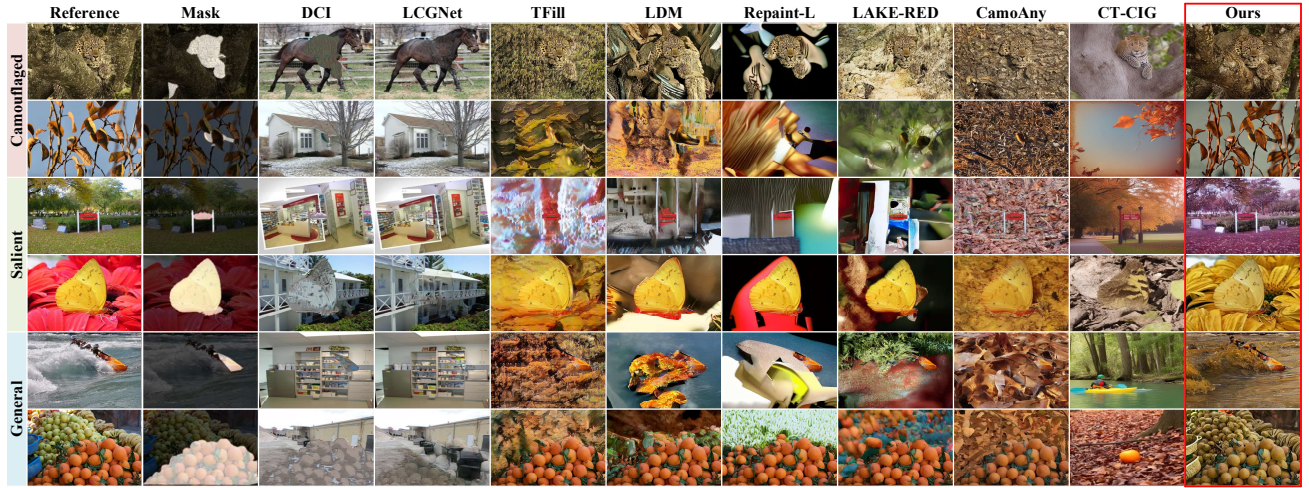


Figure 4. Qualitative comparison with existing SOTA methods including style transfer based (column 3 to 4), out-painting based (column 5 to 9), and text-driven (column 10) approaches. Our results are demonstrated in the rightmost column with red box.

Table 1. Quantitative comparison with SOTA methods on LAKE-RED datasets. The 1st, 2nd and 3rd best results are highlighted in red, green and blue. ↑ / ↓ represents the higher / lower the better. ST: Style transfer based. OP: Out-paining based. TD: Text-driven.

Method	Type	Camouflaged Objects (6,473)				Salient Objects (6,473)				General Objects (6,473)				Overall (19,419)			
		FID↓	KID↓	SSIM↑	KL _{BF} ↓	FID↓	KID↓	SSIM↑	KL _{BF} ↓	FID↓	KID↓	SSIM↑	KL _{BF} ↓	FID↓	KID↓	SSIM↑	KL _{BF} ↓
Original	—	—	—	—	1.0027	—	—	—	2.4837	—	—	—	1.6818	—	—	—	1.7227
AB <i>IPOL 2016</i>	ST	117.11	0.0645	0.2586	0.9200	126.78	0.0614	0.2753	1.2377	133.89	0.0645	0.2884	1.1668	120.21	0.0623	0.2741	1.1082
CI <i>TOG 2010</i>	ST	124.49	0.0662	0.2133	2.0678	136.30	0.0730	0.2117	2.2911	137.19	0.0713	0.2228	2.4039	128.51	0.0693	0.2159	2.2543
AdaIN <i>Iccv 2017</i>	ST	125.16	0.0721	0.1754	0.8821	133.20	0.0702	0.1880	1.3065	136.93	0.0714	0.2077	1.1534	126.94	0.0703	0.1904	1.1140
DCI <i>AAAI 2010</i>	ST	130.21	0.0689	0.1748	6.8849	134.92	0.0665	0.1794	5.8858	137.99	0.0690	0.2010	6.1119	130.52	0.0673	0.1850	6.2935
LCGNet <i>TMM 2023</i>	ST	129.80	0.0504	0.1760	1.6329	136.24	0.0597	0.1781	1.7395	132.64	0.0548	0.1995	1.9137	129.88	0.0550	0.1845	1.7621
TFill <i>CVPR 2022</i>	OP	63.74	0.0336	0.2527	0.3399	96.91	0.0453	0.2886	0.6743	122.44	0.0747	0.2989	0.7585	80.39	0.0438	0.2801	0.5909
LDM <i>CVPR 2022</i>	OP	58.65	0.0380	0.2390	1.0277	107.38	0.0524	0.3287	1.7082	129.04	0.0748	0.3090	1.4339	84.48	0.0488	0.2923	1.3899
RePaint-L <i>CVPR 2022</i>	OP	76.80	0.0459	0.2597	3.6712	114.96	0.0497	0.3504	4.1944	136.18	0.0686	0.3303	3.5917	96.14	0.0498	0.3135	3.8191
LAKE-RED <i>CVPR 2024</i>	OP	39.55	0.0212	0.2208	0.9191	88.70	0.0428	0.2881	1.4268	102.67	0.0555	0.2736	1.4216	64.27	0.0355	0.2608	1.2558
FACIG <i>ICME 2025</i>	OP	27.61	0.0099	—	—	82.23	0.0326	—	—	96.94	0.0503	—	—	52.87	0.0229	—	—
CamoAny <i>CVPR 2025</i>	OP	32.05	0.0140	0.1591	0.2948	52.24	0.0256	0.2052	0.5905	86.35	0.0430	0.1953	0.6173	42.85	0.0233	0.1865	0.5009
CT-CIG <i>AAAI 2026</i>	TD	30.59	0.0085	0.1972	1.0199	81.60	0.0230	0.1910	1.1938	104.46	0.0241	0.2091	1.4424	52.88	0.0169	0.1991	1.2187
RealCamo (Ours)	OP	9.06	0.0015	0.3927	0.4648	11.16	0.0028	0.4670	0.9238	16.11	0.0056	0.4285	0.8365	6.93	0.0025	0.4294	0.7417

3.6. Training Objective

In RealCamo, the Stable Diffusion (SD) and the CLIP text and image encoders are all frozen, leaving ControlNet as the only trainable component. The training objective follows Equation 2, where the original control c^f is replaced by layout controls $\{c_{\text{cst}}, c_{\text{dep}}, c_{\text{hed}}\}$, and the textual condition c^t is replaced by multi-modal conditions $\{c_{\text{txt}}, c_{\text{cls}}, c_{\text{vis}}\}$. This design enables effective controllable camouflage synthesis while preserving the generalization of the pretrained SD.

3.7. Background-Foreground Distribution Divergence

To more effectively quantify the degree of camouflage in synthesized images, we propose a background–foreground distribution divergence metric, denoted as KL_{BF} , based on KL divergence. It measures visual similarity between the generated background and the foreground target via

their pixel-value distributions, where lower values indicate stronger camouflage effectiveness. Specifically, given an image I and its foreground mask M , we compute the KL divergence between background and foreground distributions for each RGB channel and average them to obtain KL_{BF} . Formally, the KL_{BF} can be calculated as:

$$\text{KL}_c = \text{KL}(I_c \cdot (1 - M), I_c \cdot M), \quad c \in \{R, G, B\}, \quad (6)$$

$$\text{KL}_{BF} = \text{Avg}(\text{KL}_R, \text{KL}_G, \text{KL}_B). \quad (7)$$

4. Experiments

4.1. Experimental Settings

Datasets and Metrics. We conduct experiments on the LAKE-RED dataset (Zhao et al., 2024), which contains 4,040 training images and 19,419 images for evaluation, including 6,473 camouflaged, salient, and general images,

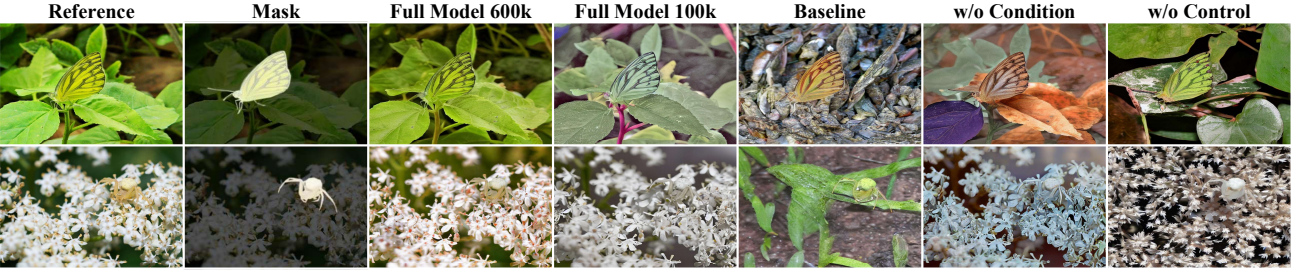


Figure 5. Qualitative results of ablation study on main components of our proposed RealCamo framework.

Table 2. Quantitative results of ablation study on main components. The best results are highlighted in **bold**. \uparrow / \downarrow represents the higher / lower the better. For layout controls, \times means only a foreground target with white background is used, without depth and HED controls. For textual-visual condition, \times means only simple textual prompt is used, without additional visual tokens.

Configuration		Camouflaged Objects (2,000)				Salient Objects (2,000)				General Objects (2,000)				Overall (6,000)			
Layout Controls	Textual-Visual Condition	FID \downarrow	KID \downarrow	SSIM \uparrow	KL $_{BF} \downarrow$	FID \downarrow	KID \downarrow	SSIM \uparrow	KL $_{BF} \downarrow$	FID \downarrow	KID \downarrow	SSIM \uparrow	KL $_{BF} \downarrow$	FID \downarrow	KID \downarrow	SSIM \uparrow	KL $_{BF} \downarrow$
\times	\times	46.52	0.0149	0.1446	0.7371	73.38	0.0266	0.2002	1.5530	102.35	0.0340	0.1953	1.3155	46.21	0.0212	0.1800	1.2019
\checkmark	\times	37.59	0.0121	0.2910	0.4019	43.97	0.0151	0.3525	0.9349	61.92	0.0280	0.3160	0.8637	27.71	0.0162	0.3198	0.7335
\times	\checkmark	32.98	0.0099	0.1712	0.7405	55.01	0.0137	0.2320	1.5997	87.27	0.0237	0.2186	1.3464	33.14	0.0106	0.2073	1.2289
\checkmark	\checkmark	31.77	0.0071	0.3254	0.3398	35.61	0.0083	0.4027	0.8659	44.90	0.0143	0.3695	0.7938	20.30	0.0083	0.3659	0.6665

Table 3. Quantitative results of ablations on layout controls. The best results are highlighted in **bold**. \uparrow / \downarrow represents the higher / lower the better.

Configuration			Overall (6,000)			
Contrast	Depth	HED	FID \downarrow	KID \downarrow	SSIM \uparrow	KL $_{BF} \downarrow$
\checkmark	\times	\times	32.99	0.0118	0.1917	0.6343
\checkmark	\checkmark	\times	25.30	0.0104	0.2887	0.6994
\checkmark	\times	\checkmark	25.54	0.0102	0.2949	0.6957
\checkmark	\checkmark	\checkmark	20.30	0.0083	0.3659	0.6665

respectively. Following Zhao et al. (2024), we adopt FID (Binkowski et al., 2018) and KID (Heusel et al., 2017) to assess the overall quality of generated images. In addition, SSIM (Wang et al., 2004) is employed to measure structural consistency between generated images and their original references, while our proposed KL_{BF} metric is used to quantify the effectiveness of visual camouflage.

Implementation Details. The proposed framework is built upon Stable Diffusion 1.5 (Rombach et al., 2022) augmented with ControlNet (Agrawala, 2023). During training, all input images, control conditions, and corresponding masks are resized to 512×512 , and a batch size of 4 is used. We set the control scale to 1.0 and train the model for 600,000 iterations with a learning rate of $1e-5$. The generated images are also in a resolution of 512×512 and are resized to their original size for evaluation. All experiments are conducted on a single NVIDIA L20 GPU.

4.2. Comparison with the State-of-the-arts (SOTAs)

We compare our RealCamo with 12 SOTAs, including five style transfer based methods (AB (Martino et al., 2016), CI

Table 4. Quantitative results of ablations on textual-visual condition. The best results are highlighted in **bold**. \uparrow / \downarrow represents the higher / lower the better. *Simple*: The simple textual prompt. *Detailed*: The unified fine-grained textual task description.

Configuration		Overall (6,000)			
Textual	Visual	FID \downarrow	KID \downarrow	SSIM \uparrow	KL $_{BF} \downarrow$
<i>Simple</i>	\times	46.21	0.0212	0.1800	1.2019
<i>Detailed</i>	\times	27.71	0.0162	0.3198	0.7335
	\checkmark	33.14	0.0106	0.2073	1.2289
<i>Detailed</i>	\checkmark	20.30	0.0083	0.3659	0.6665

(Chu et al., 2010), AdaIN (Huang & Belongie, 2017), DCI (Zhang et al., 2020), and LCGNet (Li et al., 2022b)), six out-painting based methods (TFill (Zheng et al., 2022), LDM (Rombach et al., 2022), RePaint-L (Lugmayr et al., 2022), LAKE-RED (Zhao et al., 2024), FACIG (Chen et al., 2025), and CamoAny (Das & Gopalakrishnan, 2025)), and one recently text-driven method (CT-CIG (Qian et al., 2025)). We re-evaluate the benchmark results provided by LAKE-RED and CT-CIG. Due to a lack of available resources, we reproduce CamoAny with the same settings as ours, and directly copy the results from the original paper for FACIG.

Qualitative Comparison. Fig. 4 shows qualitative comparison between our proposed RealCamo and other methods on camouflaged, salient, and generic objects. The style transfer based LCGNet embeds targets into given backgrounds, achieving strong visual camouflage but severely altering target semantics. In contrast, out-painting based methods often produce insufficient camouflage or cluttered, semantically implausible backgrounds, degrading realism. Although recent text-driven CT-CIG generates visually convincing re-

Table 5. Performance of MVANet (Yu et al., 2024a) on four COD benchmark datasets with different training data. The best results are highlighted in **bold**. \uparrow / \downarrow represents the higher / lower the better. Original: The traditional COD training data. Gen *SOD&GOD*: Synthesis images by RealCamo of the salient and general subsets in LAKE-RED evaluation set. Gen *COD*: Synthesis images by RealCamo of the LAKE-RED training set (*i.e.*, our constructed **SynCOD12K** dataset).

Training Data	CHAMELEON (76)					CAMO (250)					COD10K (2,026)					NC4K (4,121)				
	$S_\alpha \uparrow$	$E_\phi \uparrow$	$F_\beta \uparrow$	$F_\beta^w \uparrow$	$M \downarrow$	$S_\alpha \uparrow$	$E_\phi \uparrow$	$F_\beta \uparrow$	$F_\beta^w \uparrow$	$M \downarrow$	$S_\alpha \uparrow$	$E_\phi \uparrow$	$F_\beta \uparrow$	$F_\beta^w \uparrow$	$M \downarrow$	$S_\alpha \uparrow$	$E_\phi \uparrow$	$F_\beta \uparrow$	$F_\beta^w \uparrow$	$M \downarrow$
Original	0.915	0.929	0.871	0.846	0.022	0.870	0.896	0.842	0.809	0.055	0.882	0.917	0.828	0.792	0.025	0.886	0.910	0.855	0.820	0.038
Gen <i>SOD&GOD</i>	0.905	0.927	0.846	0.796	0.031	0.826	0.842	0.760	0.717	0.079	0.865	0.896	0.784	0.719	0.035	0.879	0.897	0.821	0.769	0.048
Gen <i>COD</i>	0.924	0.949	0.889	0.871	0.019	0.882	0.916	0.856	0.826	0.049	0.896	0.934	0.850	0.818	0.021	0.891	0.919	0.860	0.824	0.037

sults, they fail to preserve original targets and thus require re-annotation, limiting their usefulness for downstream COD tasks. In comparison, our RealCamo achieves both high visual similarity and strong foreground–background semantic consistency while preserving target integrity, resulting in more realistic and practically valuable camouflaged images.

Quantitative Comparison. Quantitative results are summarized in Tab. 1. Compared to early style transfer based methods, latest out-painting based and text-driven approaches achieve obviously better image quality, indicated by lower FID and KID. Owing to the introduction of explicit layout controls and textual–visual multi-modal conditioning, our RealCamo attains highly competitive generation performance. Although it does not achieve the lowest KL_{BF} score, our method balances visual camouflage with structural and semantic fidelity, producing more realistic images. By revisiting Fig. 4, methods with lower KL_{BF} values (*e.g.*, CamoAny and TFill) indeed yield stronger visual camouflage, further validating our proposed KL_{BF} as an effective metric for quantifying camouflage effectiveness.

User Study. We further conduct a user study to comprehensively evaluate the quality of synthesized camouflaged images based on human feedback. Detailed experimental settings, evaluation criteria, and statistical results and analyses will be reported in Appendix C.

4.3. Ablation Study

We conduct ablation studies to validate the proposed components. Due to computational constraints, all variants are trained for 100,000 iterations, and evaluation is performed on 6,000 images uniformly sampled from three test subsets. Results in Tab. 2 and Fig. 5 show that explicit layout controls improve structural consistency and overall image quality, supporting our claim that “*the semantics of images are largely determined by their structural layout*”. Incorporating textual–visual condition further enhances visual realism, as well as foreground–background visual similarity and semantic consistency. Additional results of ablations on individual layout control and textual–visual components are reported in Tabs 3 and 4. More quantitative and qualitative result with further analyses will be provided in Appendix.

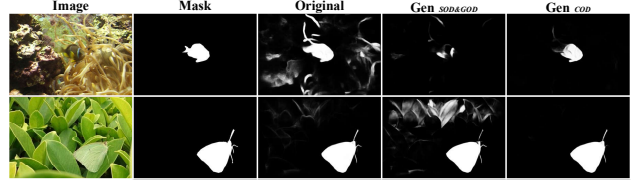


Figure 6. Prediction results with different training data.

4.4. Downstream Application

We further evaluate the impact of synthesized camouflaged images on downstream COD application. An awesome dichotomous segmentation model, MVANet (Yu et al., 2024a), is trained with different data configurations and evaluated on four COD benchmarks. Quantitative results and prediction results are presented in Tab. 5 and Fig. 6. We can observe that, converting salient or general images into camouflaged ones degrades COD performance, possibly due to domain gaps between these synthesized samples and real COD data. In contrast, training with camouflaged-synthesis images consistently improves COD performance, highlighting the effectiveness of our generation approach for data augmentation. We also examine the impact of synthesized images on salient and general object detection. More details of experimental settings, metrics and results, and the constructed **SynCOD12K** dataset, will be reported in Appendix.

5. Conclusion

In this paper, we propose RealCamo, a unified framework for controllable camouflaged image generation. RealCamo explicitly incorporates additional layout controls to regulate the structural composition of generated images, thereby enhancing semantic consistency between foreground objects and synthesized backgrounds. In addition, it constructs a multi-modal textual–visual condition by combining unified fine-grained textual task descriptions with texture-oriented background retrieved visual cues, which jointly guides the generation process to improve visual quality and realism. Extensive experiments and qualitative analyses validate the effectiveness of the proposed framework and demonstrate its strong potential for enhancing downstream camouflaged object detection applications.

References

Achanta, R., Hemami, S., Estrada, F., and Susstrunk, S. Frequency-tuned salient region detection. In *CVPR*, pp. 1597–1604, 2009. [12](#)

Agrawala, L. Z. A. R. M. Adding conditional control to text-to-image diffusion models. In *ICCV*, pp. 3836–3847, 2023. [3, 4, 7, 13](#)

Binkowski, M., Sutherland, D. J., Arbel, M., and Gretton, A. Demystifying mmd gans. In *ICLR*, 2018. [7](#)

Borji, A., Cheng, M.-M., Jiang, H., and Li, J. Salient object detection: A benchmark. *IEEE Trans. Image Process.*, 24(12):5706–5722, 2015. [12](#)

Chen, P.-C., Yi, Y., Hsu, C.-F., Xie, H., Chen, H.-J., Shuai, H.-H., and Cheng, W.-H. Foreground focus: Enhancing coherence and fidelity in camouflaged image generation. In *ICME*, 2025. [3, 7](#)

Chu, H.-K., Hsu, W.-H., Mitra, N. J., Cohen-Or, D., Wong, T.-T., and Lee, T.-Y. Camouflage images. *ACM Trans. Graph.*, 29(4):51–1, 2010. [3, 7](#)

Cong, R., Sun, M., Zhang, S., Zhou, X., Zhang, W., and Zhao, Y. Frequency perception network for camouflaged object detection. In *ACM MM*, pp. 1179–1189, 2023. [12](#)

Das, B. and Gopalakrishnan, V. Camouflage anything: Learning to hide using controlled out-painting and representation engineering. In *CVPR*, pp. 3603–3613, 2025. [1, 3, 4, 5, 7](#)

Diederik, P. K. and Max, W. Auto-encoding variational bayes. In *ICLR*, 2014. [13](#)

Esser, P., Rombach, R., and Ommer, B. Taming transformers for high-resolution image synthesis. In *CVPR*, pp. 12873–12883, 2021. [3](#)

Everingham, M., Gool, L. V., Williams, C. K., Winn, J., and Zisserman, A. The pascal visual object classes (voc) challenge. *IJCV*, 88(2):303–338, 2010. [1](#)

Fan, D.-P., Cheng, M.-M., Liu, Y., Li, T., and Borji, A. Structure-measure: A new way to evaluate foreground maps. In *ICCV*, pp. 4558–4567, 2017. [12](#)

Fan, D.-P., Gong, C., Cao, Y., Ren, B., Cheng, M.-M., and Borji, A. Enhanced-alignment measure for binary foreground map evaluation. In *IJCAI*, pp. 698–704, 2018. [12](#)

Fan, D.-P., Ji, G.-P., Sun, G., Cheng, M.-M., Shen, J., and Shao, L. Camouflaged object detection. In *CVPR*, pp. 2774–2784, 2020. [1, 12](#)

Fan, D.-P., Ji, G.-P., Cheng, M.-M., and Shao, L. Concealed object detection. *IEEE Trans. Pattern Anal. Mach. Intell.*, 44(10):6024–6042, 2022. [12](#)

Goodfellow, I., Pouget-Abadie, J., Mirza, M., Xu, B., Warde-Farley, D., Ozair, S., Courville, A., and Bengio, Y. Generative adversarial networks. *Commun. ACM*, 63(11):139–144, 2020. [2](#)

Guan, J., Fang, X., Zhu, T., Cai, Z., Ling, Z., Yang, M., and Luo, J. Idenet: Making neural network identify camouflaged objects like creatures. *IEEE Trans. Image Process.*, 33:4824–4839, 2024. [12](#)

He, C., Li, K., Zhang, Y., Tang, L., Zhang, Y., Guo, Z., and Li, X. Camouflaged object detection with feature decomposition and edge reconstruction. In *CVPR*, pp. 22046–22055, 2023. [12](#)

He, C., Li, K., Zhang, Y., Zhang, Y., You, C., Guo, Z., Li, X., Danelljan, M., and Yu, F. Strategic preys make acute predators: Enhancing camouflaged object detectors by generating camouflaged objects. In *ICLR*, 2024. [12](#)

He, C., Zhang, R., Xiao, F., Fang, C., Tang, L., Zhang, Y., Kong, L., Fan, D.-P., Li, K., and Farsiu, S. Run: Reversible unfolding network for concealed object segmentation. *ICML*, 2025. [1, 12](#)

Heusel, M., Ramsauer, H., Unterthiner, T., Nessler, B., and Hochreiter, S. Gans trained by a two time-scale update rule converge to a local nash equilibrium. *NeurIPS*, 30, 2017. [7](#)

Ho, J., Jain, A., and Abbeel, P. Denoising diffusion probabilistic models. *NeurIPS*, 33:6840–6851, 2020. [2, 12](#)

Hu, E. J., Shen, Y., Wallis, P., Allen-Zhu, Z., Li, Y., Wang, S., Wang, L., and Chen, W. Lora: Low-rank adaptation of large language models. *ICLR*, 2022. [3](#)

Huang, X. and Belongie, S. Arbitrary style transfer in real-time with adaptive instance normalization. In *ICCV*, pp. 1501–1510, 2017. [7](#)

Huang, Z., Dai, H., Xiang, T.-Z., Wang, S., Chen, H.-X., Qin, J., and Xiong, H. Feature shrinkage pyramid for camouflaged object detection with transformers. In *CVPR*, pp. 5557–5566, 2023. [12](#)

Ji, G.-P., Fan, D.-P., Chou, Y.-C., Dai, D., Liniger, A., and Gool, L. V. Deep gradient learning for efficient camouflaged object detection. *Mach. Intell. Res.*, 20(1):92–108, 2023. [12](#)

Jia, Q., Yao, S., Liu, Y., Fan, X., Liu, R., and Luo, Z. Segment, magnify and reiterate: Detecting camouflaged objects the hard way. In *CVPR*, pp. 4713–4722, 2022. [12](#)

Kim, A. R. J. W., Hallacy, C., Ramesh, A., Goh, G., Agarwal, S., Sastry, G., Askell, A., Mishkin, P., Clark, J., Krueger, G., and Sutskever, I. Learning transferable visual models from natural language supervision. In *ICML*, pp. 8748–8763, 2021. 3

Kupyn, O., Kataoka, H., and Rupprecht, C. S3od: Towards generalizable salient oobject detection with synthetic data. *arXiv preprint arXiv:2510.21605*, 2025. 2

Le, T.-N., Nguyen, T. V., Nie, Z., Tran, M.-T., and Sugimoto, A. Anabranch network for camouflaged object segmentation. *Comput. Vis. Image Underst.*, 184:45–56, 2019. 12

Li, D., Ling, H., Kim, S. W., Kreis, K., Fidler, S., and Torralba, A. Bigdatasetgan: Synthesizing imagenet with pixel-wise annotations. In *CVPR*, pp. 21330–21340, 2022a. 3

Li, Y., Zhai, W., Cao, Y., and Zha, Z.-J. Location-free camouflage generation network. *IEEE Trans. Multimed.*, 25:5234–5247, 2022b. 2, 3, 7

Lin, T.-Y., Maire, M., Belongie, S., Hays, J., Perona, P., Ramanan, D., Dollár, P., and Zitnick, C. L. Microsoft coco: Common objects in context. In *ECCV*, pp. 740–755, 2014. 1

Long, J., Shelhamer, E., and Darrell, T. Fully convolutional networks for semantic segmentation. In *CVPR*, pp. 3431–3440, 2015. 12

Lugmayr, A., Danelljan, M., Romero, A., Yu, F., Timofte, R., and Gool, L. V. Repaint: Inpainting using denoising diffusion probabilistic models. In *CVPR*, pp. 11461–11471, 2022. 7

Lv, Y., Zhang, J., Dai, Y., Li, A., Liu, B., Barnes, N., and Fan, D.-P. Simultaneously localize, segment and rank the camouflaged objects. In *CVPR*, pp. 11586–11596, 2021. 1, 12

Margolin, R., Zelnik-Manor, L., and Tal, A. How to evaluate foreground maps? In *CVPR*, pp. 248–255, 2014. 12

Martino, J. M. D., Facciolo, G., and Meinhardt-Llopis, E. Poisson image editing. *Image Process. Line*, 6:300–325, 2016. 7

Mei, H., Ji, G.-P., Wei, Z., Yang, X., Wei, X., and Fan, D.-P. Camouflaged object segmentation with distraction mining. In *CVPR*, pp. 8768–8777, 2021. 12

Mumuni, A., Mumuni, F., and Gerrar, N. K. A survey of synthetic data augmentation methods in machine vision. *Mach. Intell. Res.*, 21(5):831–869, 2024. 3

Pang, Y., Zhao, X., Xiang, T.-Z., Zhang, L., and Lu, H. Zoom in and out: A mixed-scale triplet network for camouflaged object detection. In *CVPR*, pp. 2150–2160, 2022. 12

Perazzi, F., Krähenbühl, P., Pritch, Y., and Hornung, A. Saliency filters: Contrast based filtering for salient region detection. In *CVPR*, pp. 733–740, 2012. 12

Qian, Y., Chen, H., Li, W., Liu, N., and j. Qin. Text-guided controllable diffusion for realistic camouflage images generation. *arXiv preprint arXiv:2511.20218*, 2025. 3, 5, 7

Qin, C., Zhang, S., Yu, N., Feng, Y., Yang, X., Zhou, Y., Wang, H., Niebles, J. C., Xiong, C., Savarese, S., Ermon, S., Fu, Y., and Xu, R. Unicontrol: A unified diffusion-model for controllable visual generation in the wild. In *NeurIPS*, 2023. 3, 4

Raffel, C., Shazeer, N., Roberts, A., Lee, K., Narang, S., Matena, M., Zhou, Y., Li, W., and Liu, P. J. Exploring the limits of transfer learning with a unified text-to-text transformer. *J. Mach. Learn. Res.*, 21(140):1–67, 2020. 3

Rezende, D. J., Mohamed, S., and Wierstra, D. Stochastic backpropagation and approximate inference in deep generative models. In *ICML*, pp. 1278–1286, 2014. 3, 13

Rombach, R., Blattmann, A., Lorenz, D., Esser, P., and Ommer, B. High-resolution image synthesis with latent diffusion models. In *CVPR*, pp. 10684–10695, 2022. 2, 3, 4, 7, 12, 13

Sharma, P. K., Matiyali, N., Srivastava, S., and Sharma, G. Preserve anything: Controllable image synthesis with object preservation. In *ICCV*, pp. 18058–18067, 2025. 3

Skurowski, P., Abdulameer, H., Błaszczyk, J., Depta, T., Kornacki, A., and Kozięł, P. Animal camouflage analysis: Chameleon database. *Unpublished manuscript*, 2(6):7, 2018. 12

Song, Z., Kang, X., Wei, X., Liu, H., Dian, R., and Li, S. Fsnet: Focus scanning network for camouflaged object detection. *IEEE Trans. Image Process.*, 32:2267–2278, 2023. 12

Sun, Y., Wang, S., Chen, C., and Xiang, T.-Z. Boundary-guided camouflaged object detection. In *IJCAI*, pp. 1335–1341, 2022. 12

Sun, Y., Xu, C., Yang, J., Xuan, H., and Luo, L. Frequency-spatial entanglement learning for camouflaged object detection. In *ECCV*, pp. 343–360, 2025. 12

Wang, C.-Y., Ji, G., Shao, S., Cheng, M.-M., and Fan, D.-P. Context-measure: Contextualizing metric for camouflage. *arXiv preprint arXiv:2512.07076*, 2025. 2

Wang, Q., Yang, J., Yu, X., Wang, F., Chen, P., and Zheng, F. Depth-aided camouflaged object detection. In *ACM MM*, pp. 3297–3306, 2023. [12](#)

Wang, Z., Bovik, A. C., Sheikh, H. R., and Simoncelli, E. P. Image quality assessment: from error visibility to structural similarity. *IEEE Trans. Image Process.*, 13(4): 600–612, 2004. [7](#)

Wu, W., Zhao, Y., Shou, M. Z., Zhou, H., and Shen, C. Diffumask: Synthesizing images with pixel-level annotations for semantic segmentation using diffusion models. In *ICCV*, pp. 1206–1217, 2023a. [3](#)

Wu, Z., Paudel, D. P., Fan, D.-P., Wang, J., Wang, S., Demonceaux, C., Timofte, R., and Gool, L. V. Source-free depth for object pop-out. In *ICCV*, pp. 1032–1042, 2023b. [12](#)

Xiao, F., Hu, S., Shen, Y., Fang, C., Huang, J., He, C., Tang, L., Yang, Z., and Li, X. A survey of camouflaged object detection and beyond. *CAAI Artif. Intell. Res.*, 2024. [1](#), [12](#)

Xie, C., Xia, C., Yu, T., and Li, J. Frequency representation integration for camouflaged object detection. In *ACM MM*, pp. 1789–1797, 2023. [12](#)

Xie, S. and Tu, Z. Holistically-nested edge detection. In *ICCV*, pp. 1395–1403, 2015. [5](#)

Xu, Y., He, Z., Shan, S., and Chen, X. Ctrlora: An extensible and efficient framework for controllable image generation. In *ICLR*, 2025. [3](#)

Yang, L., Kang, B., Huang, Z., Zhao, Z., Xu, X., Feng, J., and Zhao, H. Depth anything v2. In *NeurIPS*, 2024. [5](#)

Yin, B., Zhang, X., Fan, D.-P., Jiao, S., Cheng, M.-M., Gool, L. V., and Hou, Q. Camoformer: Masked separable attention for camouflaged object detection. *IEEE Trans. Pattern Anal. Mach. Intell.*, 46(12):10362–10374, 2024. [12](#)

Yu, Q., Zhao, X., Pang, Y., Zhang, L., and Lu, H. Multi-view aggregation network for dichotomous image segmentation. In *CVPR*, pp. 3921–3930, 2024a. [8](#)

Yu, Z., Zhang, X., Zhao, L., Bin, Y., and Xiao, G. Exploring deeper! segment anything model with depth perception for camouflaged object detection. In *ACM MM*, pp. 4322–4330, 2024b. [12](#)

Zhai, Q., Li, X., Yang, F., Chen, C., Cheng, H., and Fan, D.-P. Mutual graph learning for camouflaged object detection. In *CVPR*, pp. 12997–13007, 2021. [12](#)

Zhang, Q., Yin, G., Nie, Y., and Zheng, W.-S. Deep camouflage images. In *AAAI*, volume 34, pp. 12845–12852, 2020. [3](#), [7](#)

Zhang, Y., Ling, H., Gao, J., Yin, K., Lafleche, J.-F., Barriuso, A., Torralba, A., and Fidler, S. Datasetgan: Efficient labeled data factory with minimal human effort. In *CVPR*, pp. 10145–10155, 2021. [3](#)

Zhao, P., Xu, P., Qin, P., Fan, D.-P., Zhang, Z., Jia, G., Zhou, B., and Yang, J. Lake-red: Camouflaged images generation by latent background knowledge retrieval-augmented diffusion. In *CVPR*, pp. 4092–4101, 2024. [1](#), [2](#), [3](#), [4](#), [5](#), [6](#), [7](#), [12](#)

Zheng, C., Cham, T.-J., Cai, J., and Phung, D. Bridging global context interactions for high-fidelity image completion. In *CVPR*, pp. 11512–11522, 2022. [7](#)

Zhou, T., Zhou, Y., Gong, C., Yang, J., and Zhang, Y. Feature aggregation and propagation network for camouflaged object detection. *IEEE Trans. Image Process.*, 31: 7036–7047, 2022. [12](#)

A. Camouflage Object Detection

A.1. Related Work

As the extension of general object detection (GOD) (Long et al., 2015) and salient object detection (SOD) (Borji et al., 2015), camouflaged object detection (COD) (Fan et al., 2020; He et al., 2025) is proposed to accurately localize and precisely segment camouflaged targets hidden within complex scenes, which is applicable to numerous real-world scenarios, such as concealed defect detection in industry, pest monitoring in agriculture, and medical lesions diagnosis (Xiao et al., 2024). SINet (Fan et al., 2020) pioneered COD using a biologically inspired two-stage search-and-identify framework, followed by a wide range of bio-inspired (Mei et al., 2021; Fan et al., 2022; Pang et al., 2022; Jia et al., 2022; Song et al., 2023; Guan et al., 2024) and feature-enhanced (Zhai et al., 2021; Lv et al., 2021; Zhou et al., 2022; Huang et al., 2023; He et al., 2024; Yin et al., 2024) methods. Subsequent studies incorporated auxiliary cues to complement RGB images, including edges and textures (Sun et al., 2022; Ji et al., 2023; He et al., 2023), depth information (Wu et al., 2023b; Wang et al., 2023; Yu et al., 2024b), and frequency-domain representations (Xie et al., 2023; Cong et al., 2023; Sun et al., 2025). Representative works exploit frequency decomposition with boundary refinement (He et al., 2023), depth-induced saliency enhancement (Wu et al., 2023b), and joint frequency–spatial learning (Sun et al., 2025). Despite steady progress, the development of COD remains fundamentally limited by the small scale of available training datasets, which drives the development of camouflaged image generation tasks.

A.2. Datasets and Evaluation Metrics

Datasets. We evaluate the effectiveness of our synthetic dataset, *SynCOD12K*, on the COD task following the standard practice of SINet (Fan et al., 2020). Experiments are conducted on four widely used benchmark datasets: *CHAMELEON* (Skurowski et al., 2018), *CAMO* (Le et al., 2019), *COD10K* (Fan et al., 2020), and *NC4K* (Lv et al., 2021). The *CHAMELEON* dataset contains 76 images, while *CAMO* consists of 1,250 images across 8 classes. *COD10K* includes 5,066 images spanning ten super-classes, and *NC4K* serves as the largest testing benchmark with 4,121 well-annotated images. For standard COD training, we follow the common practice by using 1,000 images from *CAMO* and 3,040 images from *COD10K* as the training set, which also aligns with the training protocol for camouflaged image generation in (Zhao et al., 2024). The remaining images from these two datasets, together with all images from *CHAMELEON* and *NC4K*, are used for evaluation.

Evaluation Metrics. To thoroughly evaluate the performance, we adopt five standard metrics widely used in COD and SOD tasks: mean absolute error (M) (Perazzi et al., 2012), mean E-measure (E_ϕ) (Fan et al., 2018), mean F-measure (F_β) (Achanta et al., 2009), weighted F-measure (F_β^w) (Margolin et al., 2014), and structure measure (S_α) (Fan et al., 2017). Better performance is indicated by lower values of M and higher values of E_ϕ , F_β , F_β^w , and S_α .

B. Preliminary

B.1. Diffusion Models

Tex-to-image (T2I) generation methods, represented by Stable Diffusion (Rombach et al., 2022), synthesize images conditioned on textual descriptions (c^t) via a denoising diffusion paradigm (Ho et al., 2020). These models can operate either in pixel space or latent space, with latent diffusion models (Rombach et al., 2022) offering substantially improved computational efficiency.

Forward Process. In diffusion models, noise sampled from the Gaussian distribution $\epsilon \sim \mathcal{N}(0, I)$ is progressively added to a clean image x_0 , resulting in a noisy sample x_t at timestep t :

$$x_t = \sqrt{\bar{\alpha}_t} x_0 + \sqrt{1 - \bar{\alpha}_t} \epsilon, \quad (8)$$

where $\alpha_t = 1 - \beta_t$, $\bar{\alpha}_t = \prod_{s=1}^t \alpha_s$, and $\{\beta_t\}$ follows a variance schedule.

Training Objective. A denoising network ϵ_θ is trained to predict the injected noise ϵ by minimizing the following objective:

$$\mathcal{L} = \mathbb{E}_{x_0, t, \epsilon \sim \mathcal{N}(0, I)} [\| \epsilon - \epsilon_\theta(x_t, t, c^t) \|_2^2]. \quad (9)$$

Reverse Process. After training the denoising network, an image x_0 can be gradually obtained by repeating the denoise

operation T times on an entire Gaussian noise $x_T \sim \mathcal{N}(0, I)$, following:

$$x_{t-1} = \frac{1}{\sqrt{\bar{\alpha}_t}} \left(x_t - \frac{\beta_t}{\sqrt{1 - \bar{\alpha}_t}} \epsilon_\theta(x_t, t, c^t) \right) + \sigma_t \epsilon', \quad (10)$$

where t starts from T , $\epsilon' \sim \mathcal{N}(0, I)$, and $\sigma_t^2 = \beta_t$. Intermediate estimations of x_0 can also be directly obtained at any timestep t following:

$$\hat{x}_0 = \frac{x_t - \sqrt{1 - \bar{\alpha}_t} \epsilon_\theta(x_t, t, c^t)}{\sqrt{\bar{\alpha}_t}}. \quad (11)$$

In latent diffusion models (LDMs) (Rombach et al., 2022), the above forward and reverse process is conducted on latent embeddings $z = \mathcal{E}_{\text{VAE}}(x)$, as a latent representation of raw RGB pixels x encoded by a VAE (Diederik & Max, 2014; Rezende et al., 2014). And the denoised latent representation z_0 is further decoded into a normal RGB image using the VAE decoder, as $x_0 = \mathcal{D}_{\text{VAE}}(z_0)$.

B.2. ControlNet

ControlNet (Agrawala, 2023) remarkably extends the controllability of large pretrained T2I LDMs by incorporating addition conditions (c^f) like Canny edges, human pose, or depth map, which provide structural priors for the target generated image.

Architecture. ControlNet controls the generating process by injecting additional conditions into the blocks of a pretrained neural network. With the definition $\mathcal{F}(\cdot; \Theta)$ of a trained neural block with parameters Θ , that transform an input feature map x into an output feature map y as $y = \mathcal{F}(x; \Theta)$, a trainable copy of \mathcal{F} is created as $\mathcal{F}_c(\cdot; \Theta_c)$.

This trainable copy takes an external conditioning vector c^f as input, and is connected to the locked model \mathcal{F} with zero convolution layers $\mathcal{Z}(\cdot; \cdot)$, which are 1×1 convolution layers with both weight and bias initialized to zeros. The ControlNet then generated the output y_c by two instances of zero convolutions with parameters Θ_{Z1} and Θ_{Z2} as:

$$y_c = \mathcal{F}(x; \Theta) + \mathcal{Z}(\mathcal{F}(x + \mathcal{Z}(c^f; \Theta_{Z1}); \Theta_c); \Theta_{Z2}) \quad (12)$$

Training Objective. With the introduction of additional conditioning vector c^f , the overall training objective (Equation 9) is reformulated as:

$$\mathcal{L} = \mathbb{E}_{x_0, t, c^t, c^f, \epsilon \sim \mathcal{N}(0, I)} [\| \epsilon - \epsilon_\theta(x_t, t, c^t, c^f) \|_2^2]. \quad (13)$$

This enables fine-grained spatial control during generation, allowing precise alignment between generated content and structural constraints.

C. User Study

The results are currently being collected and pending further analysis..